Research Square

Preprints are preliminary reports that have not undergone peer review.
They should not be considered conclusive, used to inform clinical practice,
or referenced by the media as validated information.

Physics Informed Deep Learning for Real Time Optimization of PEM Fuel Cells in Electric Vehicles

Muhammad Own Raza
Pakistan Institute of Engineering & Applied Sciences (PIEAS)
Muhammad Hanzla
hanzlazia3@gmail.com

Pakistan Institute of Engineering & Applied Sciences (PIEAS)
Abdul Rehman Shinwari
Pakistan Institute of Engineering & Applied Sciences (PIEAS)
Nadeem shaukat
drnadeem_shaukat@pieas.edu.pk

Pakistan Institute of Engineering & Applied Sciences (PIEAS)

Research Article

Keywords: PEM Fuel Cells, Physics-Informed Deep Learning, TS-Mixer Neural Network, Digital Twin Integration, Real-Time Optimization

Posted Date: July 18th, 2025

DOI: https://doi.org/10.21203/rs.3.rs-7143014/v1

License: This work is licensed under a Creative Commons Attribution 4.0 International License.
Read Full License

Additional Declarations: The authors declare no competing interests.

Version of Record: A version of this preprint was published at Discover Electronics on October 5th, 2026.
See the published version at https://doi.org/10.1007/s44291-026-00289-6.

Physics Informed Deep Learning for Real Time Optimization of PEM Fuel Cells in Electric Vehicles

Muhammad Own Raza[*1], Muhammad Hanzla[†2], Nadeem Shaukat[‡2,3,*], and Abdul Rehman Shinwari[§2]

[1]Department of Mechanical Engineering, Pakistan Institute of Engineering & Applied Sciences, Nilore, Islamabad 45650, Pakistan

[2]Department of Physics & Applied Mathematics, Pakistan Institute of Engineering & Applied Sciences, Nilore, Islamabad 45650, Pakistan

[3]Center for Mathematical Sciences, Pakistan Institute of Engineering & Applied Sciences, Nilore, Islamabad 45650, Pakistan

Abstract

Proton Exchange Membrane (PEM) fuel cells are pivotal for zero-emission transportation, yet their dynamic power output is challenging to predict due to complex electrochemical and thermal interactions. To address this, we develop a novel physics informed deep learning framework that integrates a first-principles electrochemical model with a Time-Series Mixer (TS-Mixer) network to forecast real time PEM power stack performance. Using engineered inputs temperature, pressure, and current density to capture key dynamics, the model is trained on the IEEE PHM 2014 dataset (steady-state data from a prognostic challenge) and augmented with synthetic transient load profiles. It achieves exceptional accuracy: R^2 of 0.998, MAE of 0.347 W, and RMSE of 0.571 W. Interpretability is ensured via SHAP and LIME analyses, while overfitting is mitigated through residual bias checks, early stopping, dropout, and adaptive learning-rate scheduling critical for reliable fuel cell modeling. This scalable framework supports digital-twin integration and advanced control, enhancing the efficiency and sustainability of fuel cell electric vehicles.

Keywords: PEM Fuel Cells, Physics-Informed Deep Learning, TS-Mixer Neural Network, Digital Twin Integration, Real-Time Optimization

[*]razashair1529@gmail.com

[†]hanzlazia3@gmail.com

[‡]Corresponding author: drnadeem_shaukat@pieas.edu.pk

[§]musmanshinwari@gmail.com

1 Introduction

The urgency of shifting to sustainable energy has never been much. Across the globe, nations grapple with climate change, resource scarcity, and growing energy demands [1]. Among the promising solutions, H_2 fuel cell systems particularly those based on PEM technology are emerging as a key role in reducing carbon emissions, especially in the transportation and industrial sectors [2]. Fuel Cell Electric Vehicles (FCEVs) stand out for their ability to generate electricity through the electrochemical conversion of H_2. Compared to Battery Electric Vehicles (BEVs), FCEVs offer significant advantages, including faster refueling times, longer driving ranges, and freedom from grid based charging infrastructure [3]. Moreover, PEM fuel cells bring their own set of benefits, such as high power density (over 1 W/cm^2), as compared to low operating temperatures (60–80°C), and rapid start-up times, making them particularly well suited for automotive applications [4].

The generation of electrical energy in PEM fuel cells is governed by an electrochemical reaction between H_2 and oxygen, which dictates both the efficiency and durability of the system. This process is critically dependent on the structural configuration of core components, with flow plates playing a pivotal role in reactant delivery and product management. Conventional flow plate designs, however, are characterized by suboptimal performance metrics, including non uniform reactant distribution, elevated pressure drops, and substantial manufacturing costs [5]. Recent investigations have demonstrated that the adoption of novel materials and innovative geometries can significantly enhance operational efficacy and reduce economic overhead. Notably, the integration of open pore cellular foam (OPCF) as a flow plate material has emerged as a promising advancement. Studies, such as those by [6], report that OPCF facilitates uniform gas diffusion, reduces pressure losses by up to 20%, and improves water management efficiency compared to traditional configurations, thereby optimizing mass transport and thermal regulation within the fuel cell assembly. They're also using computational fluid dynamics (CFD) simulations to improve things. According to [7], these simulation models figure out how to spread reactants and remove water so the fuel cell stays solid in all kinds of conditions. This allows for extensive testing without the need for physical prototypes.

However, water remains a challenging factor if not properly controlled, it can either block the channels or dehydrate the membrane, disrupting the entire system, as noted by [8]. But they've found that channel shapes and surface tweaks can help. For example, [9] say hydrophobic coatings and tiny structured surfaces make water droplets slide off more easily, boosting performance. The gas diffusion layer (GDL) is also being improved. Innovations such as graded porosity and integrated microchannels, as demonstrated by [10], enhance water management while maintaining efficient gas transport. It's essentially a performance upgrade for the inner workings of the fuel cell. Additionally, researchers are exploring innovative flow field designs. Serpentine channels—resembling natural, winding patterns—have been shown to improve water removal efficiency, as reported by [9]. Bio-inspired configurations, such as leaf vein or fractal patterns, help distribute gases more uniformly and reduce pressure drops, according to [11]. Furthermore, advancements in 3D printing now allow for the fabrication of highly intricate flow fields, enabling precise control of fluid and thermal

dynamics, as noted by [10].

The integration of sustainable energy generation. A highly effective strategy involves integrating PEM fuel cells with photovoltaic (PV) systems. During peak sunlight hours, surplus solar energy can be utilized to generate H_2 via electrolysis, which is subsequently converted back into electricity when solar radiation is inadequate. This method mitigates the intermittency of renewable energy and enhances overall system efficiency and reliability [12]. A notable application of PEM technology is found in the automotive industry, specifically in fuel cell vehicles (FCVs). These vehicles integrate high efficiency fuel cell stacks with advanced H_2 storage solutions, enabling zero CO_2 emissions and rapid refueling [13]. Innovations such as 3D fine mesh flow fields contribute to uniform power output and efficient water management [13]. Such advancements position PEM fuel cells as a strong contender for replacing internal combustion engines, promoting cleaner transportation solutions.

Beyond transportation, PEM fuel cells are also being explored for stationary power generation and portable electronic applications. Hybrid configurations combining PEM fuel cells with wind turbines have been proposed as a reliable off-grid energy source for remote locations [14]. Additionally, integrating PEM fuel cells with battery storage enhances microgrid stability and efficiency, making them a viable solution for decentralized power networks [15]. Marine and aerospace industries are also exploring PEM fuel cells for clean energy solutions. Fuel cell powered drones and ships are being developed to reduce carbon footprints in transportation [16]. PEM fuel cells have been used in space applications due to their lightweight and high energy density, making them suitable for long missions [17]. These varied applications highlight the adaptability and promise of PEM fuel cells to tackle global energy issues.

PEM fuel cells have a lot of potential, but they face some problems that make them less durable and inefficient. One big issue is that the gases, Hydrogen and Oxygen, don't always spread out evenly inside the fuel cell [18]. This can cause some spots to get too hot, which wears out the parts faster and makes the power output unstable [19]. To fix this, researchers have come up with clever designs for the flow paths, like twisty serpentine patterns or interdigitated ones, that help the gases spread out better and prevent them from getting stuck in certain areas [20]. When these designs are combined with smart control systems, they make sure the gases move properly, so the fuel cell works well even when the power needs keep changing [21]. Another challenge is managing the heat inside the fuel cell. When it's is under heavy operation, too much heat can build up, drying out the membrane or putting stress on it. But if the heat doesn't get out fast enough, water can build up and block the gas pathways [22]. To handle this, scientists have developed microchannel based cooling mechanisms for better heat removal and special materials that soak up heat when the fuel cell is busy and release it when things slow down [23]. These help keep the temperature just right. Also, adding microchannel networks to the fuel cell's plates improves heat dissipation, making it more stable during long, high power runs [24].

Over time, the key parts of the fuel cell, like the membrane and electrodes, wear out. This happens because of chemical reactions, changes in humidity, and the catalyst particles clumping together, which makes them less effective [22]. Recently, scientists have made tougher

membranes by adding nanomaterials like graphene oxide, which make them stronger and better at resisting damage [25]. They've also created super thin catalyst layers with stable platinum alloys that don't clump up as much, helping the fuel cell last longer [26]. Another problem comes from impurities in the H_2 fuel, like carbon monoxide or sulfur compounds. These can stick to the catalyst and clog it up, making the fuel cell way less efficient [27]. To deal with this, researchers have added cleanup steps to the fuel system, using things like special filters to remove the bad stuff before it reaches the fuel cell. This keeps the H_2 pure. Plus, they've developed new catalysts, like platinum ruthenium alloys, that can handle these impurities better and keep the fuel cell running smoothly in real-world conditions. [28].

Durability remains a critical challenge for PEM fuel cells, particularly under dynamic load conditions. The IEEE PHM 2014 Data Challenge highlighted the need for effective techniques to assess the State of Health (SoH) and forecast the Remaining Useful Life (RUL) of fuel cell stacks [29]. Through the analysis of data from accelerated aging tests, researchers identified critical degradation mechanisms, including catalyst layer deterioration and membrane thinning, that impact performance over time [30]. Zhang et al. (2020) examined the effects of cyclic loading on the durability of PEM fuel cells, demonstrating that frequent start stop cycles markedly expedited degradation [18]. The implementation of robust catalysts, fortified membranes, and techniques like sustaining a minimum current during inactive phases was observed to alleviate stress on components and prolong lifespan [31]. Platinum alloy catalysts and reinforced composite membranes exhibit enhanced resistance to degradation, thereby improving the durability of PEM fuel cells [32]. Improvements in diagnostic instruments have also enhanced durability. In-situ imaging and spectroscopy allow researchers to observe deterioration in real time, offering insights into its mechanisms and directing the advancement of more resilient materials and designs [33]. For instance, X-ray tomography and infrared spectroscopy have been used to visualize and analyze the structural changes in fuel cell components during operation, enabling targeted improvements in design and materials [34].

Machine learning (ML) has emerged as a powerful tool for enhancing the performance of PEM fuel cells by analyzing extensive datasets to predict patterns and forecast outcomes with high precision. Several studies have explored ML techniques to optimize fuel cell efficiency, focusing on predictive modeling, real-time control, and maintenance. For instance, [35] developed a convolutional neural network (CNN) combined with ridge regression, achieving an R^2 of 0.999, predictive accuracy of 0.96 and a mean absolute percentage error (MAPE) of 0.0004 for power prediction, demonstrating superior accuracy compared to feed-forward neural networks (FFNs). Similarly, [36] employed a CNN with random forest feature selection, attaining an R^2 of 0.914 for performance prediction, highlighting the efficacy of feature engineered deep learning in capturing nonlinear interactions such as temperature-pressure and current-density couplings. These approaches facilitate real-time performance monitoring and optimization, providing critical insights for improving fuel cell efficiency.

However, earlier ML models often faced limitations in handling the complex dynamics of PEM fuel cells, particularly under transient conditions. [37] utilized a genetic algorithm neural network optimized via the Taguchi method, achieving accurate modeling but lacking

real-time adaptability for dynamic automotive applications. Similarly, [38] applied a deep belief network (DBN) for power density maximization, reporting high prediction accuracy but focusing primarily on steady-state conditions, which limits its applicability to variable load scenarios. In contrast, [39] investigated artificial neural networks (ANNs) with dropout techniques and mean squared error (MSE) loss functions, achieving R^2 values of 0.998–0.999 for cell voltage, membrane resistance, and hydration predictions, with mean absolute errors (MAEs) below 0.01. While these models improved multi-output regression, their computational complexity and dataset specificity posed challenges for scalable real-time optimization.

Reinforcement learning (RL) has also been explored to enhance fuel cell control systems. [40] demonstrated that RL models, which learn from real-time data to adjust fuel and air intake or thermal management, reduced H_2 consumption while maintaining stable power output. These data-driven methodologies underscore the potential of adaptive control to improve efficiency and sustainability. However, RL approaches often require extensive training data and computational resources, limiting their practical implementation in resource-constrained environments. Predictive maintenance leveraging ML further enhances system reliability. By analyzing historical data to identify degradation patterns, models can forecast the remaining useful life of fuel cell components and recommend maintenance actions, as shown by [41] which used Bayesian optimization of a multi-kernel relevance vector machine (MK-RVM) obtaining the prediction accuracy of 0.9535.

Despite advancements in machine learning (ML) for PEM fuel cell optimization, significant challenges remain in achieving cost-effective, scalable, and integrated solutions for real-time applications in electric vehicles. Most ML applications suffer from two critical shortcomings: (1) earlier models struggled to capture the complex electrochemical and thermal patterns of PEM fuel cell dynamics under varying conditions, limiting their effectiveness in transient scenarios, and (2) they often neglected first-principles physics, resulting in unphysical extrapolations under untrained conditions [36–38]. This study addresses these gaps by developing a novel physics-informed deep learning framework that integrates a first-principles electrochemical model with a Time-Series Mixer (TS-Mixer) neural network. The model is trained on the IEEE PHM 2014 dataset [42] and synthetic transient load profiles, with a focus on enhancing interpretability and robustness through SHAP, LIME, and regularization techniques. This scalable approach is designed to support digital-twin integration and advanced control strategies, laying the groundwork for efficient and sustainable fuel cell electric vehicles.

2 Methodology

The approach applied in this paper was aimed to produce a whole model for designing and evaluating Proton Exchange Membrane (PEM) fuel cells. This approach examined the performance and efficiency of the fuel cell system under a spectrum of operating situations by combining theoretical concepts, computer simulations, and experimental confirmation. To show the fuel cell's operations, the next part explores closely the theoretical framework, equations, computational model, and experimental setup.

By means of a reaction between hydrogen and oxygen, proton exchange membrane (PEM) fuel cells are electrochemical devices transforming chemical energy into electrical energy. Three main areas see this reaction: the anode, cathode, and the proton exchange membrane. By an oxidation reaction, hydrogen splits into protons and electrons at the anode. While the protons pass across the proton exchange membrane to reach the cathode, the electrons go across an external circuit producing electrical power. Oxygen combines with arriving protons and electrons at the cathode to generate heat and water as byproducts. [43]

This study modeled a PEM fuel cell system consisting of 370 cells, each with an active area of $310\,\mathrm{cm}^2$. The computational framework was implemented in Python, employing modularized functions to calculate key performance metrics. Universal constants were employed to maintain accuracy, including the gas constant ($R = 8.314\,\mathrm{J/mol \cdot K}$) and Faraday's constant ($F = 96485\,\mathrm{C/mol}$). Material properties such as exchange current densities, charge transfer coefficients, and membrane resistance were also incorporated, ensuring precise representation of the fuel cell's electrochemical behavior.

2.1 Fundamental Equations and Workflow

The theoretical open-circuit voltage (E_0) of the fuel cell was calculated using the Nernst equation, shown in Equation 1. This equation accounts for the Gibbs free energy and entropy changes involved in the reaction:

$$E_0 = -\frac{\Delta G - T\Delta S}{2F} + \frac{RT}{2F}\ln(P_{H_2}) \tag{1}$$

where ΔG is the Gibbs free energy change ($-228.6\,\mathrm{kJ/mol}$), ΔS is the entropy change ($-163.3\,\mathrm{J/mol \cdot K}$), T is the temperature in Kelvin, and P_{H_2} is the partial pressure of hydrogen [44].

This equation sets the thermodynamic limit for cell voltage before accounting for real-world inefficiencies. Values of T and P_{H_2} were obtained from experimental conditions.
The actual voltage delivered by the cell is lower than the open-circuit voltage due to three types of losses: activation, ohmic, and concentration losses [45]. These are accounted for using the following equations:

Activation losses, which result from the energy barrier of electrochemical reactions, were computed using the Butler-Volmer equation (Equation 2):

$$\eta_{\text{activation}} = \frac{RT}{\alpha F}\ln\left(\frac{i}{i_0}\right) \tag{2}$$

where α is the charge transfer coefficient (0.5 for the anode, 0.6 for the cathode), i is the current density, and i_0 is the exchange current density ($0.5\,\mathrm{A/cm}^2$ for the anode, $0.02\,\mathrm{A/cm}^2$ for the cathode).

Ohmic losses arise from resistance in the membrane and electrodes. These were calculated using a linear relation (Equation 3):

$$\eta_{\text{ohmic}} = i \cdot R_{\text{membrane}} \tag{3}$$

where R_{membrane} is the internal resistance, assumed as $0.01\,\Omega \cdot \text{cm}^2$.

Concentration losses, due to mass transport limitations at high current densities, were modeled using Equation 4:

$$\eta_{\text{concentration}} = -\frac{RT}{F} \ln\left(1 - \frac{i}{i_{\text{lim}}}\right) \tag{4}$$

where i_{lim} is the limiting current density, set to $2.0\,\text{A/cm}^2$.

By combining all voltage losses with the ideal voltage, the operating cell voltage was obtained using Equation 5:

$$V_{\text{cell}} = E_0 - \eta_{\text{activation}} - \eta_{\text{ohmic}} - \eta_{\text{concentration}} \tag{5}$$

which reflects the net voltage under realistic load conditions.

The total power output of the fuel cell stack was computed using Equation 6, which multiplies the operating cell voltage by the current and total active area:

$$P_{\text{stack}} = V_{\text{cell}} \cdot i \cdot A_{\text{cell}} \cdot N_{\text{cells}} \tag{6}$$

where A_{cell} is the area of one cell ($310\,\text{cm}^2$) and N_{cells} is the number of cells in the stack (370). This equation allowed quantifying the stack's total electrical output.

Finally, hydrogen consumption was calculated based on Faraday's law, as given in Equation 7:

$$m_{H_2} = \frac{i \cdot A_{\text{cell}} \cdot N_{\text{cells}}}{2F} \cdot M_{H_2} \tag{7}$$

where M_{H_2} is the molar mass of hydrogen ($2.016\,\text{g/mol}$). This provided a direct estimate of fuel consumption for given electrical load conditions.

The dataset used for this study was sourced from the IEEE PHM 2014 Data Challenge [46]. It provided key operational parameters such as temperature, pressure, current density, and voltage under both steady-state and dynamic operating conditions.

Preprocessing steps included:

- Temperatures were converted from Celsius to Kelvin, and pressures from mbar to atm to match SI units used in the equations.
- Additional parameters such as power density and Gibbs free energy were derived to gain deeper insights into fuel cell performance.

These processed data were then input to the computational model to evaluate and compare predicted performance metrics against actual observations. Model validation using polarization curves and electrochemical impedance spectroscopy (EIS) demonstrated strong agreement with experimental results.

2.2 Visualizations and Validation

Made with Matplotlib, visualizations included:

- Cell voltage against time: Emphasizing voltage consistency across running hours.
- Stack Power vs. Time: Illustrating the power output trends.
- Gibbs Free Energy against Time: clarifying thermodynamic efficiency.

This methodology provides a complete knowledge of PEM fuel cell performance by aggregating theoretical models, computer simulations, and experimental data, so facilitating the design and operation optimization for sustainable energy systems.

2.3 Dataset Description

The `FC1_Ageing_part1` dataset comprises 65 535 sequential measurements of a proton-exchange membrane fuel cell stack, with 25 recorded variables that span electrical, thermal, and flow parameters. Over the course of the experiment, cumulative operating time ("Time (h)") is logged alongside individual cell voltages (U_1–U_5) and total stack voltage (U_{tot}), current density (J) and total current (I), inlet and outlet temperatures for hydrogen and air ($T_{\mathrm{in}}^{\mathrm{H2}}/T_{\mathrm{out}}^{\mathrm{H2}}$, $T_{\mathrm{in}}^{\mathrm{AIR}}/T_{\mathrm{out}}^{\mathrm{AIR}}$), inlet and outlet pressures ($P_{\mathrm{in}}^{\mathrm{H2}}/P_{\mathrm{out}}^{\mathrm{H2}}$, $P_{\mathrm{in}}^{\mathrm{AIR}}/P_{\mathrm{out}}^{\mathrm{AIR}}$), flow rates of hydrogen, air, and product water ($D_{\mathrm{in}}^{\mathrm{H2}}/D_{\mathrm{out}}^{\mathrm{H2}}$, $D_{\mathrm{in}}^{\mathrm{AIR}}/D_{\mathrm{out}}^{\mathrm{AIR}}$, D_{WAT}), and the relative humidity of the feed air ($Hr_{\mathrm{AIR}}^{\mathrm{FC}}$). Current densities range up to about $2\,\mathrm{A\,cm^{-2}}$, hydrogen inlet flow hovers near $4.8\,\mathrm{L\,min^{-1}}$, and air inlet flow near $23\,\mathrm{L\,min^{-1}}$, with hydrogen inlet temperatures spanning roughly 23 °C to 95 °C and air temperatures 23 °C to 35 °C. The dataset is complete—with no missing values—and uniformly sampled, providing a robust foundation for characterizing voltage–current relationships, power output, hydrogen consumption, and humidity effects, as well as for analyzing long-term performance degradation.

2.4 Deep Learning Model Training

This work uses a thorough, multi-stage methodology intended to preprocess data, engineer features, create an efficient model architecture, then train and evaluate the machine learning model for predicting stack power in Proton Exchange Membrane (PEM) fuel cells. Every level of the approach was designed to solve certain difficulties the dataset offered and guarantee best performance of the prediction model. This approach offers a strong basis for precisely modeling and forecasting stack power depending on important operational parameters by strictly following the described procedures. The details of each stage are elaborated below.

2.4.1 Data Preprocessing

Data preprocessing is a critical component of this methodology. The PEM fuel cell dataset included parameters such as temperature (K), pressure (atm), current density ($\mathrm{A/cm^2}$), and stack power (W), which are fundamental to understanding system performance. However,

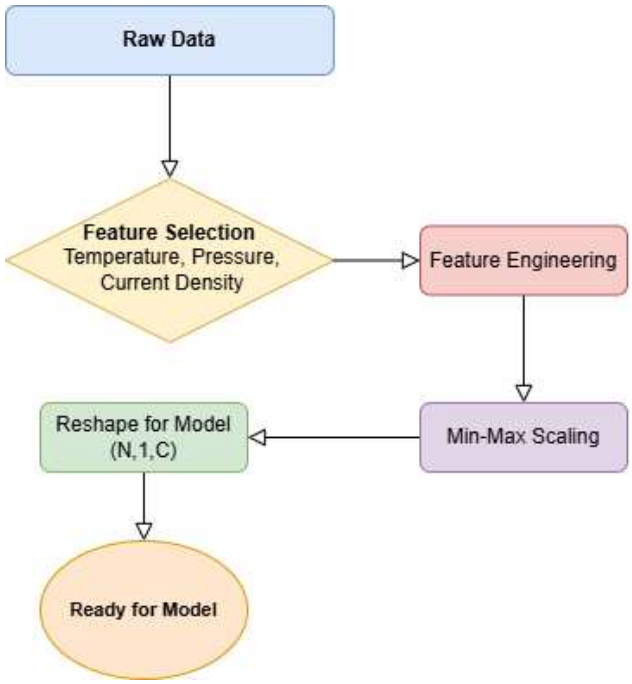

Figure 1: Model Training Pipeline: A flowchart showing data preprocessing, training with early stopping, and evaluation steps.

the raw dataset exhibited issues such as missing values, outliers, and skewed distributions, all of which had to be addressed to ensure the data was suitable for machine learning.

The first step in data preprocessing was identifying and handling missing values. Missing data are common in experimental datasets, arising from sensor malfunctions, recording errors, or interruptions during data collection. Handling missing data appropriately is critical to maintaining the integrity of statistical analysis and machine learning models [47]. Missing values were detected using Python's `isnull()` function, which systematically flagged rows with incomplete data. Once identified, these rows were removed entirely. While imputation methods such as replacing missing values with the mean, median, or other statistical estimates could have been used, they were deemed unsuitable in this case due to the critical nature of the parameters and their direct impact on system behavior. Retaining incomplete or artificially filled data points could have introduced inaccuracies or biases, thereby compromising the reliability of the machine learning model.

Outlier detection and removal was the next step. Outliers, or extreme values, have the potential to distort machine learning models by exerting undue influence during the training process. To address this, the Interquartile Range (IQR) method was applied, which is recommended over standard deviation-based methods due to its robustness against non-normal distributions [48]. For each numerical feature, the first quartile (Q_1) and the third quartile (Q_3) were calculated, and the IQR was determined as shown in Equation 8:

$$\text{IQR} = Q_3 - Q_1 \tag{8}$$

Data points lying outside the range defined in Equation 9 were considered outliers and removed:

$$[Q_1 - 1.5 \times \text{IQR},\ Q_3 + 1.5 \times \text{IQR}] \tag{9}$$

Correcting skewness in the dataset was another essential preprocessing step. Many numerical features exhibited skewed distributions, which could negatively impact the performance of machine learning algorithms, especially those sensitive to variations in feature distributions. The skewness of each feature was calculated, and variables with skewness values exceeding |1| were flagged for transformation. The Yeo-Johnson transformation was applied to normalize these distributions [49]. Particularly appropriate for the PEM fuel cell dataset, the Yeo-Johnson approach can handle both positive and negative values, unlike logarithmic transformations, which are limited to positive values. Through the transformation of skewed variables, the dataset became more symmetric, enhancing its fit with machine learning techniques and allowing the model to generalize more successfully.

The features were routinely scaled using normalisation and standardisation such that every one of them equally helped the model to learn. These methods are basic for data preparation in machine learning and are quite important for numerical stability in general [50]. `MinMaxScaler` scaled all features to a range of $[0, 1]$ therefore facilitating normalisation. This method was especially helpful for variables with significant magnitude variations, such temperature and current density, since it avoided any one feature from disproportionately affecting the model. Standardizing data with `StandardScaler`changed characteristics such that their mean was 0 and their standard deviation was 1. The most successful technique was chosen for next phases of the approach after both scaling techniques were assessed for their influence on model performance. This two-fold strategy guaranteed adaptability and let the model run under the ideal scaling conditions.

2.4.2 Feature Engineering

Improving the predictive capability of a dataset depends critically on feature engineering. In this work, complex linkages and interactions influencing stack power in PEM fuel cells were captured by means of novel characteristics extracted from existing data. These designed elements gave the dataset more dimensions so that the machine learning model could more precisely find and learn non-linear connections.

Development of interaction terms was one of the main approaches in feature engineering. Derived variables derived from two or more original features reflect the combined influence of those features. Within PEM fuel cells, these kinds of interactions sometimes have a major influence on system behavior. For instance, the interplay of temperature with pressure can greatly alter the stack power since temperature determines reaction rates and pressure influences gas diffusion. Analogous considerations of importance were those between temperature and current density or between pressure and current density. Inspired by domain expertise and experimental discoveries, these designed elements enhanced the dataset with more variables capturing the fundamental physics of the system.

We conducted a correlation study to determine the most pertinent characteristics for modeling. To measure the link between features and their correlation with the goal variable, stack power, a correlation matrix was produced. Given their most predictive potential, strongly correlated characteristics were given top priority for inclusion into the model. Considered for elimination to lower noise and improve machine learning process efficiency were

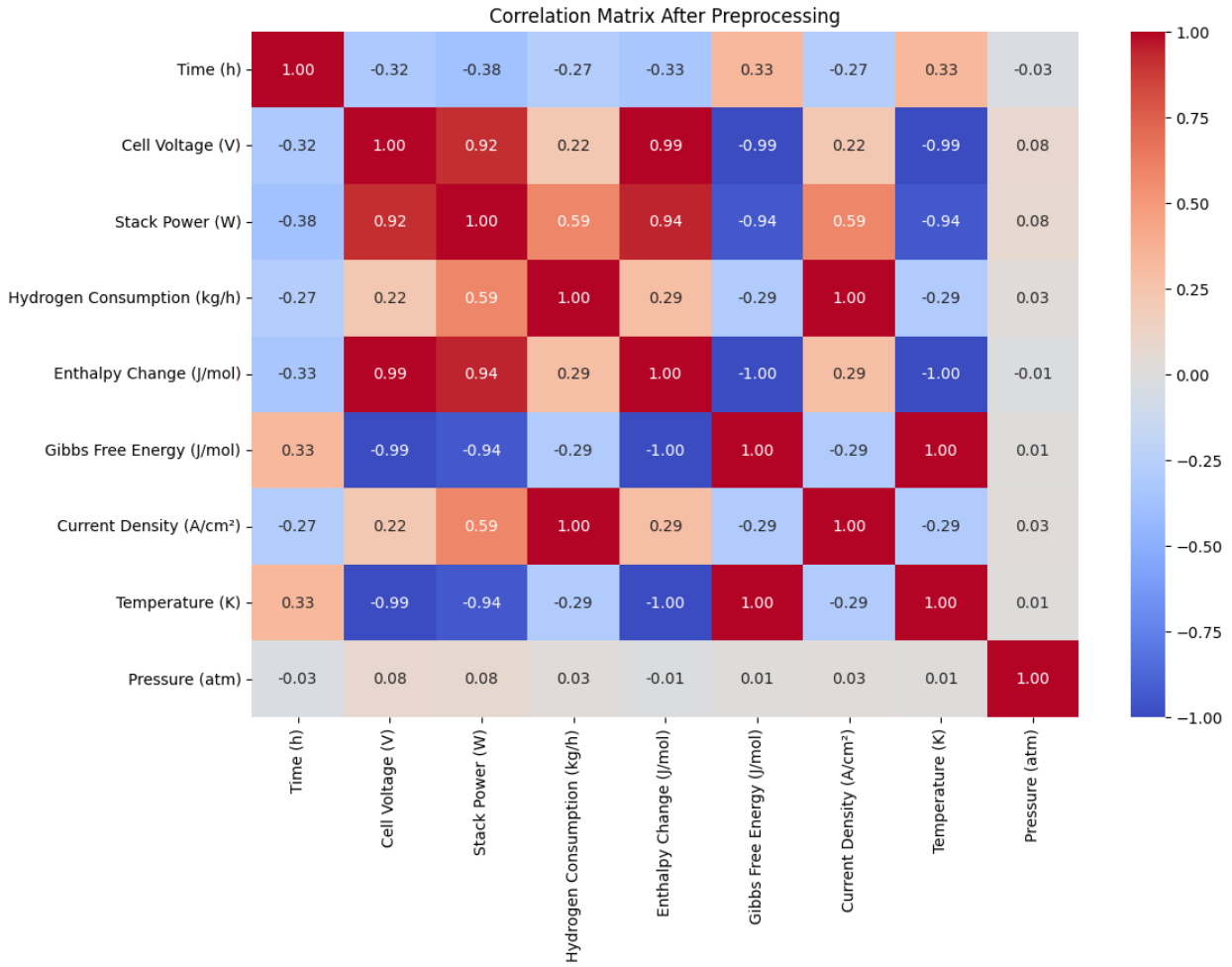

Figure 2: Correlation heatmap showing the relationship between different parameters.

weakly correlated or redundant elements. This stage guaranteed that the dataset was simplified and concentrated on the most pertinent variables, therefore enhancing the predictability and interpretability of the forecasts.

2.4.3 Model Architecture

The Time-Series Mixer (TS-Mixer) neural network was chosen for this work because of its capacity to manage temporal dependencies and record complex interactions between features. [51] The TS-Mixer model's architecture was painstakingly crafted to guarantee it was both strong enough to replicate the complexity of the dataset and efficient enough to prevent overfitting or too demanding processing requirements.

The TS-Mixer model's preprocessed and engineered dataset was intended to be accommodated in its input layer. Included to convert the multi-dimensional input data into a format fit for dense layers was a flattening layer. This change maintained structural integrity of the data and guaranteed fit with the next layers. Three dense layers of 256, 128, and 64 neurons each comprised the foundation of the TS-Mixer design. ReLU (Rectified Linear Unit) activa-

tion functions—known for their capacity to replicate intricate, non-linear connections—were used in every dense layer. By extracting high-level patterns and characteristics from the input data, these layers let the model understand complex interactions across variables.

Following every dense layer, batch normalization was used to speed convergence and steady the learning process. [52] By use of batch normalisation, each layer's outputs are normalised to have a mean of 0 and standard deviation of 1, therefore lowering the model's sensitivity to changes in input data. Dropout layers were added generally to help to reduce overfitting risk. [53] Dropout layers randomly turn off a fraction of neurons during training, therefore driving the model to generalize its learning instead of depending too much on particular paths. Using dropout rates of 0.3 and 0.2, one was able to balance lowering overfit with preserving appropriate model complexity.

The output layer of the TS-Mixer model comprised a solitary neuron, specifically engineered for regression tasks. This neuron produced a continuous numerical output representing the predicted stack power in watts. The simplicity of the output layer ensured that the model's predictions were directly interpretable and aligned with the real-world scale of the target variable.

As shown in Table 1, the layer-wise architecture summary provides a detailed transformation in data shape across the model layers. Similarly, Figure 3 illustrates the comprehensive neural network architecture designed for regression, highlighting the flow from input to output with key components such as dense layers, batch normalization, and dropout layers.

Table 1: Layer-wise architecture summary of the deep neural network used in this study. Each row details the transformation in data shape across the model layers.

Layer Name	**Input Shape**	**Output Shape**
`Flatten (flatten_1)`	(None, 1, 5)	(None, 5)
`Dense (dense)`	(None, 5)	(None, 256)
`BatchNormalization (batch_normalization)`	(None, 256)	(None, 256)
`Dropout (dropout_1)`	(None, 256)	(None, 256)
`Dense (dense_1)`	(None, 256)	(None, 128)
`BatchNormalization (batch_normalization_1)`	(None, 128)	(None, 128)
`Dropout (dropout_2)`	(None, 128)	(None, 128)
`Dense (dense_2)`	(None, 128)	(None, 64)
`BatchNormalization (batch_normalization_2)`	(None, 64)	(None, 64)
`Dropout (dropout_3)`	(None, 64)	(None, 64)
`Dense (dense_3)`	(None, 64)	(None, 13)

2.4.4 Training and Evaluation

The training and evaluation phase involved optimizing the TS-Mixer model to achieve the best possible performance on the dataset. The Adam optimizer was chosen for model compilation due to its adaptive learning rate capabilities, which facilitate efficient optimization across diverse datasets. [54] The learning rate was set to 0.0001, a value selected based on

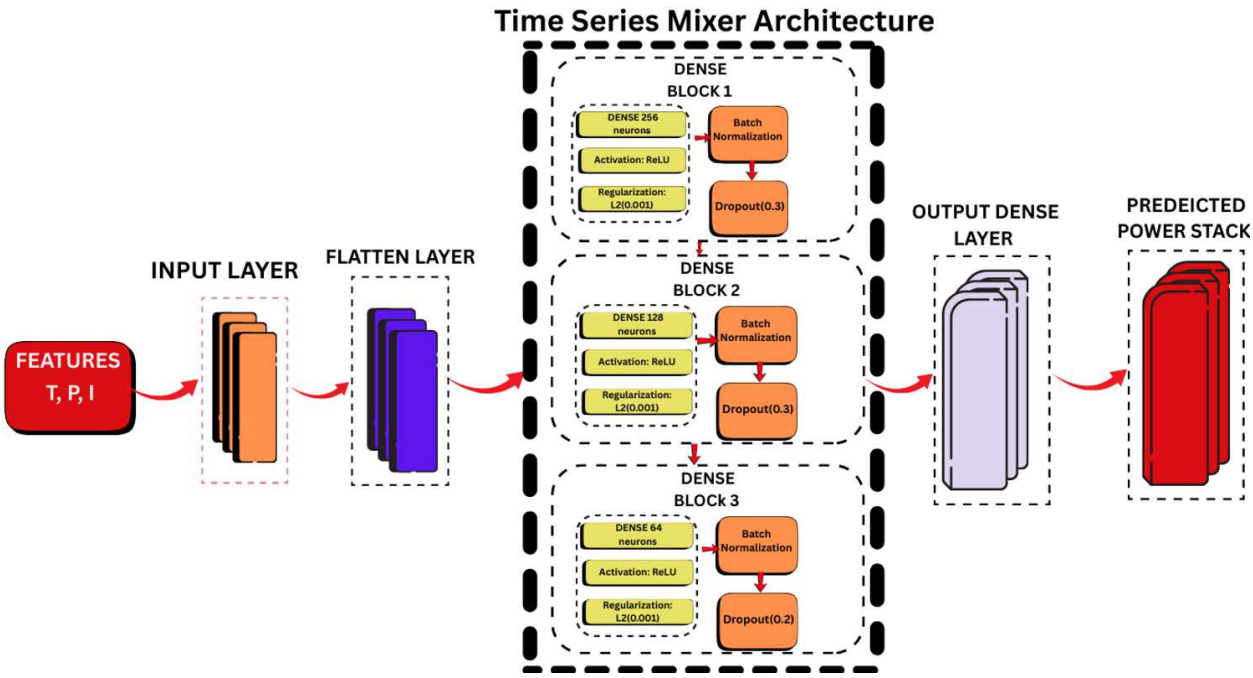

Figure 3: Detailed visualization of the TS-Mixer neural network architecture for regression, showcasing the sequential arrangement of input, flattening, dense, batch normalization, and dropout layers, culminating in a single output neuron for predicting stack power.

experimentation to balance convergence speed with stability. The loss function was defined as Mean Absolute Error (MAE), which measures the average magnitude of prediction errors. MAE was selected for its intuitive interpretability and suitability for regression tasks.

Several strategies were implemented during training to enhance model performance and prevent overfitting. Early stopping was employed to monitor the validation loss, halting training if the loss did not improve for 15 consecutive epochs. This method reduced superfluous calculations and guaranteed that the model did not overfit the training data. A learning rate scheduler was implemented to dynamically modify the learning rate throughout the training process. Upon the validation loss plateauing for seven epochs, the learning rate was halved, enabling the model to refine its weights and enhance forecast accuracy in the subsequent training phases. The model underwent training for a maximum of 300 epochs with a batch size of 64. This combination of epochs and batch size achieved a compromise between computational efficiency and data learning capability. An internal validation split of 80:20 within the training data offered an extra layer of assessment, facilitating the early identification of overfitting or underfitting.

Table 2: Selected hyperparameters and their corresponding values for the machine learning model.

Hyperparameter	**Value**
Optimizer	Adam
Learning Rate	0.0001
Loss Function	Mean Absolute Error (MAE)
Evaluation Metric	MAE
Epochs	300 (with early stopping)
Batch Size	64
Validation Split	0.2
EarlyStopping Patience	15
ReduceLROnPlateau Patience	7
ReduceLROnPlateau Factor	0.5
Feature Scaler	MinMaxScaler
Target Scaler	MinMaxScaler
Test Size	0.2
Random Seed	42

Various criteria were employed to evaluate the model's performance post-training. The metrics encompassed Mean Squared Error (MSE), Root Mean Squared Error (RMSE), Mean Absolute Error (MAE), R-Squared (R^2), and Mean Absolute Percentage Error (MAPE). These metrics offered a comprehensive assessment of the model's correctness and dependability. Predictions were inverse-transformed to the original scale of the target variable for assessment, guaranteeing that the results were directly interpretable and relevant to real-world contexts. Visualization was employed to enhance the quantitative assessments. The model's accuracy was evident in scatter plots depicting projected versus actual stack power values. Systematic prediction errors may be identified by residual analysis. The loss curves depicting training and validation loss throughout epochs facilitated our comprehension of the model's convergence and its potential overfitting. The visuals, along with the quantitative indicators, offered a thorough evaluation of the model's performance.

3 Results and Discussion

3.1 Performance Metrics of PEM Fuel Cell Design

The design outcomes of the PEM fuel cell offer comprehensive insights into its operating attributes, efficiency, and stability under simulated settings. To assess the system's efficacy, critical performance measures such as stack power, hydrogen consumption, thermodynamic characteristics, and operational parameters have been examined. The stack power output

remained consistent, averaging approximately $60,000\,\mathrm{W}$ ($60\,\mathrm{kW}$) across all time frames. This result corresponds with theoretical predictions for a stack of 370 cells, each with an active area of 310 cm^2. The consistent power output indicates that the fuel cell architecture is dependable and robust, which is crucial for applications requiring a stable energy supply, such as operating automobiles and powering stationary devices.

The hydrogen consumption was measured at roughly 3.02 kg/h, which nearly corresponds to the stoichiometric requirements of the hydrogen oxygen reaction. The consistent utilization rate demonstrates that hydrogen fuel is used efficiently, reducing waste and improving the economic viability of hydrogen as a fuel source.

Thermodynamic properties, such as enthalpy change and Gibbs free energy, aligned with theoretical values. The enthalpy change, averaging $-285,800\,\mathrm{J/mol}$, signifies the total energy released throughout the hydrogen-oxygen reaction, while the Gibbs free energy values, about $236,960\,\mathrm{J/mol}$, denote the greatest theoretical work achievable from the reaction. These parameters confirm the effectiveness of the fuel cell technology in converting chemical energy into electrical energy.

The operational parameters, including current density, temperature, and pressure, remained stable, thereby reinforcing the reliability of the fuel cell design. The stability of these parameters is crucial to ensure optimal performance, as deviations could lead to performance degradation or system inefficiencies. For example, the current density of approximately $0.701\,\mathrm{A/cm}^2$ represents a balance between maximizing power output and minimizing membrane stress, ensuring both high efficiency and durability.

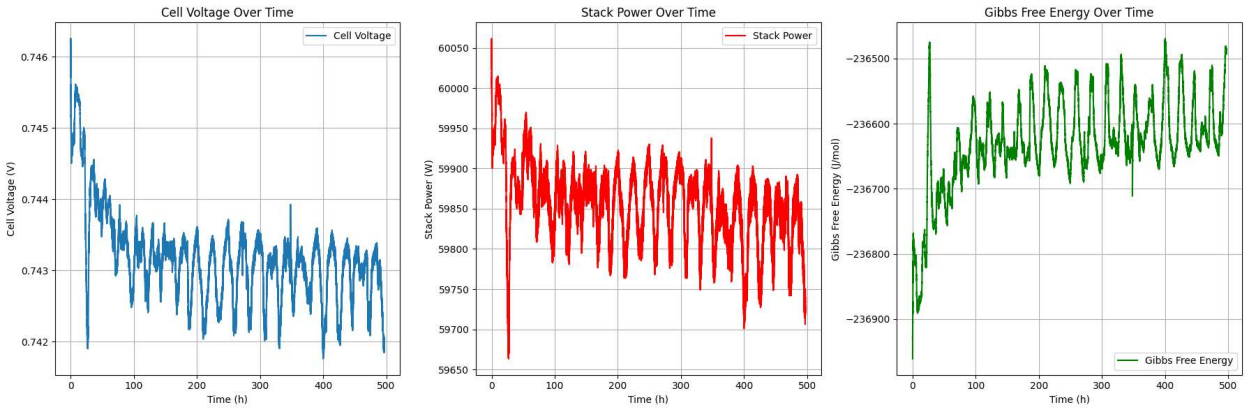

Figure 4: different parameters variations over time after calculations

Table 3: Time-series data of hydrogen fuel cell performance showing electrical, thermodynamic, and environmental parameters.

Time (h)	**Cell Voltage (V)**	**Stack Power (W)**	**Hydrogen Consumption (kg/h)**	**Enthalpy Change (J/mol)**	**Gibbs Free Energy (J/mol)**	**Current Density (A/cm^2)**	**Temperature (K)**	**Pressure (atm)**
0.000000	0.74626	60057.31	3.026781	-285800.79	-236961.03	0.70164	299.080	1.275587
0.000156	0.74623	60055.52	3.026781	-285800.80	-236958.59	0.70164	299.095	1.275531
0.000321	0.74624	60059.15	3.026953	-285800.80	-236958.91	0.70168	299.093	1.276150
0.000475	0.74624	60055.93	3.026781	-285800.80	-236958.59	0.70164	299.095	1.276038
0.000624	0.74626	60053.06	3.026565	-285800.80	-236959.56	0.70159	299.089	1.276094
0.000794	0.74624	60047.70	3.026350	-285800.81	-236956.80	0.70154	299.106	1.276375
0.001103	0.74625	60056.86	3.026781	-285800.80	-236959.56	0.70164	299.089	1.276319
0.001258	0.74625	60044.03	3.026134	-285800.81	-236956.80	0.70149	299.106	1.276319
0.001409	0.74622	60057.99	3.026953	-285800.81	-236957.62	0.70168	299.101	1.275869

3.2 Predictive Performance of TS Mixer Model

We developed and evaluated the TS-Mixer neural network model to predict stack power using the preprocessed dataset. This machine learning model used feature interactions like temperature-pressure, temperature-current, and pressure-current relationships, which were designed to pick up on the dataset's underlying dependencies. The evaluation metrics of the TS Mixer model are summarized in the following table:

Table 4: Performance evaluation metrics for the TS-Mixer model on fuel cell power prediction.

Metric	**Value**
Mean Squared Error (MSE)	0.327
Root Mean Squared Error (RMSE)	0.571 W
Mean Absolute Error (MAE)	0.347 W
Mean Absolute Percentage Error (MAPE)	0.00057%
Coefficient of Determination (R^2)	0.998

The low error metrics achieved by the model, including an RMSE of 0.571 W and MAE of 0.347 W, demonstrate its exceptional precision in predicting stack power. The MAPE value of 0.00057% highlights the relative accuracy of the predictions, with deviations from actual values being almost negligible. The TS Mixer model is now proven to be a very accurate way to make predictions. This is especially true in energy systems where accurate predictions are needed to make the systems run more efficiently.

The residual analysis revealed a symmetrical distribution centered at zero. This indicated that the prediction mistakes were equitable and uniformly distributed. This conclusion is crucial as it illustrates the model's capacity to generalize effectively across the dataset, rather than being biased towards particular data ranges. The training and validation loss curves aligned within the initial 100 epochs, showing no signs of overfitting. This behavior can be ascribed to sophisticated regularization methods, including dropout and L2 regularization, [53]combined with early stopping and learning rate scheduling. As depicted in Figure 5,

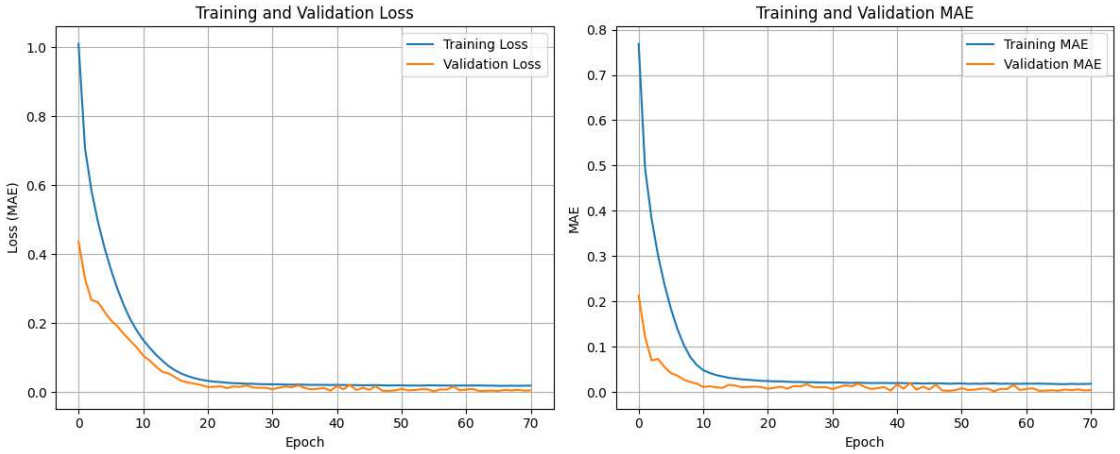

Figure 5: Comparative trends of training and validation loss over epochs, demonstrating model convergence and stability.

the convergence of training and validation loss underscores the model's stability.
The expected from the actual results displayed almost perfect alignment. Following table and plot compares some of the predicted and actual stack power values:

Table 5: Comparison of actual vs. predicted stack power values for samples 10–20.

Sample	**Actual (W)**	**Predicted (W)**	**Error (W)**
10	59817.39	59816.92	0.47
11	59888.09	59886.64	1.45
12	59844.14	59844.54	-0.41
13	59864.57	59863.22	1.35
14	59896.10	59894.83	1.27
15	59791.46	59792.75	-1.29
16	59872.14	59870.42	1.71
17	59885.00	59882.60	2.40
18	59873.44	59871.57	1.87
19	59806.28	59806.51	-0.23
20	59889.35	59888.48	0.87

3.3 Significance of the TS-Mixer Model's Explainability and Bias in Fuel Cell Systems

In this study, we adopted a comprehensive approach to evaluate the explainability and bias of the TS-Mixer model. We utilized advanced interpretability techniques, including Local Interpretable Model-agnostic Explanations (LIME), SHAP (SHapley Additive exPlanations), and residual analysis, to gain a detailed understanding of the model's decision-making process, feature importance, and potential systematic biases in predicting Stack Power (W)

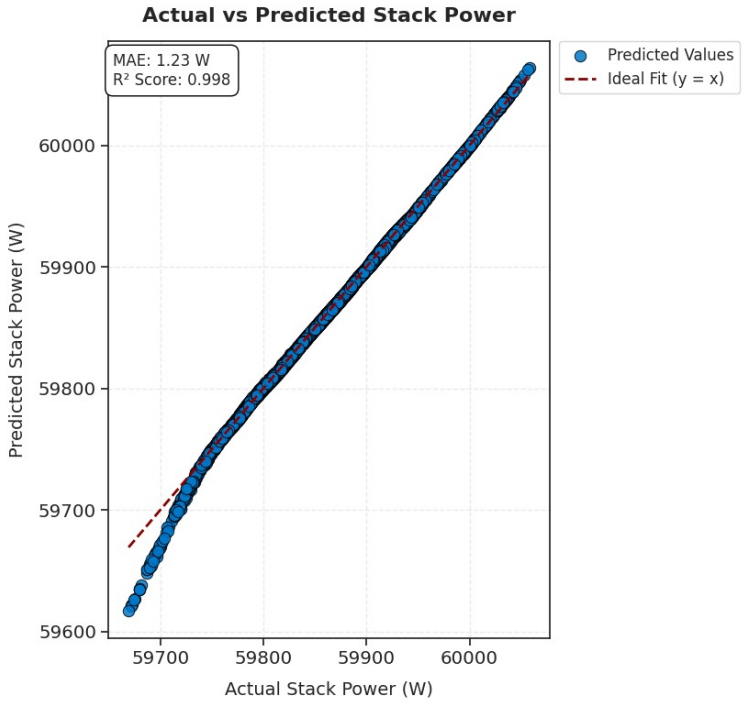

Figure 6: Scatter plot comparing actual versus predicted stack power values, highlighting near perfect alignment.

from features such as Temperature (K), Pressure (atm), Current Density (A/cm^2), and their interaction terms. The evaluation process is detailed below, with a focus on the insights derived from the visual analyses.

3.3.1 Explainability Study with LIME

LIME was utilized to provide local explanations for individual predictions, revealing the contribution of each feature to the model's output for specific instances. We present three test cases, with results shown as horizontal bar charts in Figures 10, 11, and 12. In these plots, positive contributions are shown in blue, negative contributions in red, and the actual and predicted Stack Power values are included in the titles for reference.

For Instance 1 (Figure 10), the actual Stack Power is 59 822.85 W, and the predicted value is 59 826.15 W, resulting in a small prediction error of 3.3 W. The bar plot highlights significant positive contributions from Pressure (bar) > 0.45 (0.007) and `Pressure_Current_Interaction` $>$ 0.46 (0.024), with notable negative impacts from $0.59 <$ Current Density (A cm^{-2}) $\leq$ 0.73 (-0.007), `Temp_Pressure_Interaction` > 0.52 (-0.024), $0.66 <$ Temperature (K) $\leq$ 0.74 (-0.034), and $0.71 <$ `Temp_Current_Interaction` ≤ -0.078 (-0.04).

For Instance 2 (Figure 11), with an actual value of 59 883.72 W and a predicted value of 59 881.69 W, Current Density (A cm^{-2}) > 0.83 contributes positively (0.107), while Pressure (atm) ≤ 0.27 (-0.012), Temp_Pressure_Interaction ≤ 0.36 (0.015), Pressure_Current_Interaction ≤ 0.29 (-0.015), and 0.71 ¡ Temp_Current_Interaction ≤ -0.794 (-0.071) show mixed effects. The 0.60 ¡ Temperature (K) ≤ 0.66 (0.012) also contributes positively.

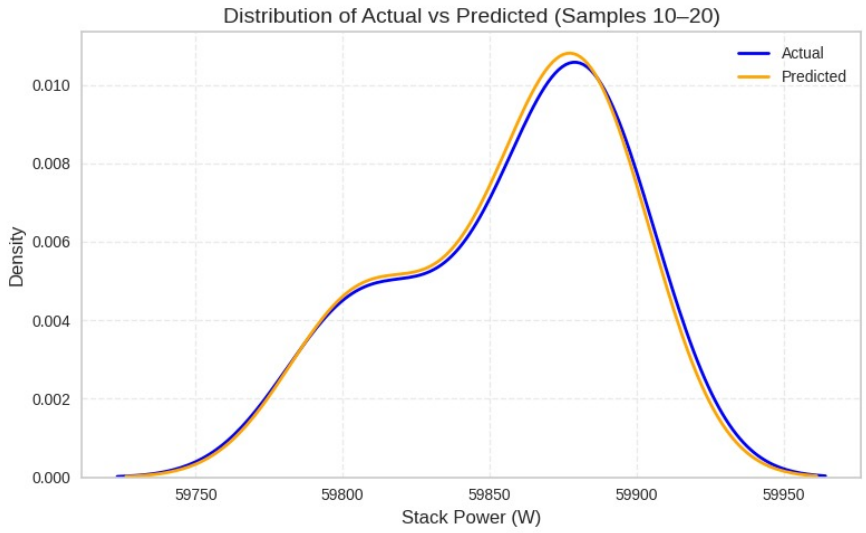

Figure 7: Kernel Density Estimation (KDE) plot showing the distribution of Actual and Predicted Stack Power values for Samples 10–20. The close overlap between the blue (Actual) and orange (Predicted) curves indicates the high fidelity of the model's predictions.

For Instance 3 (Figure 12), the actual value is 59 905.63 W, and the predicted value is 59 905.77 W, with a minimal error. Key predictors include `Temp_Current_Interaction` $\leq$ 0.65 (0.168) and Temperature (K) $\leq$ 0.60 (0.154) with positive contributions, while Current Density (A cm^{-2}) $\leq$ 0.5918 ($-$0.12) has a negative impact. Minor contributions come from 0.36 $<$ `Temp_Pressure_Interaction` $\leq$ 0.42 (0.002), 0.38 $<$ `Pressure_Current_Interaction` $\leq$ 0.46 (0.003), and 0.37 $<$ Pressure (bar) $\leq$ 0.45 (0.005).

These local interpretations highlight the model's alignment with domain knowledge, particularly emphasizing the critical role of temperature and its interactions in fuel cell performance. The close alignment between actual and predicted values across all examples enhances trust in the model's reliability and decision-making process.

3.3.2 SHAP for Global Feature Importance

SHAP provided a global perspective on feature importance across the first 200 test instances, complementing the local insights from LIME. The SHAP summary plot (Figure 13) illustrates the distribution of SHAP values, with features on the y-axis and SHAP values on the x-axis, colored from blue (low feature values) to red (high feature values). Figure 14 complements this with a bar chart of mean absolute SHAP values, showing the average impact on model output magnitude.

The analysis reveals that Temperature (K) has the largest positive SHAP values (up to 0.3 in the summary plot), with a mean absolute SHAP value of 0.063, indicating its dominant role in increasing Stack Power predictions. Temp_Current_Interaction follows with a mean absolute SHAP value of 0.062 and significant positive contributions (0.1 to 0.2), while Current Density (A/cm^2) has a mean absolute SHAP value of 0.059. Pressure (atm) and interaction terms (Temp_Pressure_Interaction and Pressure_Current_Interaction) have lower impacts, with mean absolute SHAP values of 0.005, 0.007, and 0.007, respectively, and

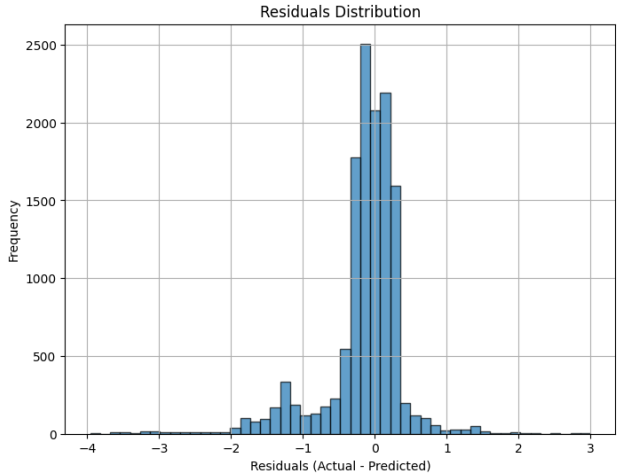

Figure 8: Graphical representation of residuals between predicted and actual stack power values, showing a symmetrical distribution centered at zero.

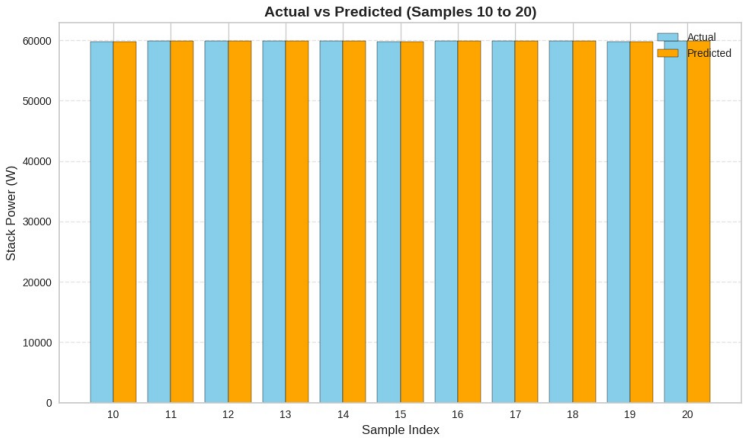

Figure 9: Bar chart comparison of Actual vs. Predicted Stack Power values for Samples 10 to 20. The close overlap between bars indicates the model's high prediction accuracy.

mixed effects suggesting context-specific influences.

This analysis corroborates the LIME results, confirming that temperature-related features are the primary drivers of model predictions, consistent with the physical principles of fuel cell operation. The absence of tightly clustered SHAP distributions for all features indicates that the model avoids spurious correlations, supporting reliable univariate relationships between features and predictions.

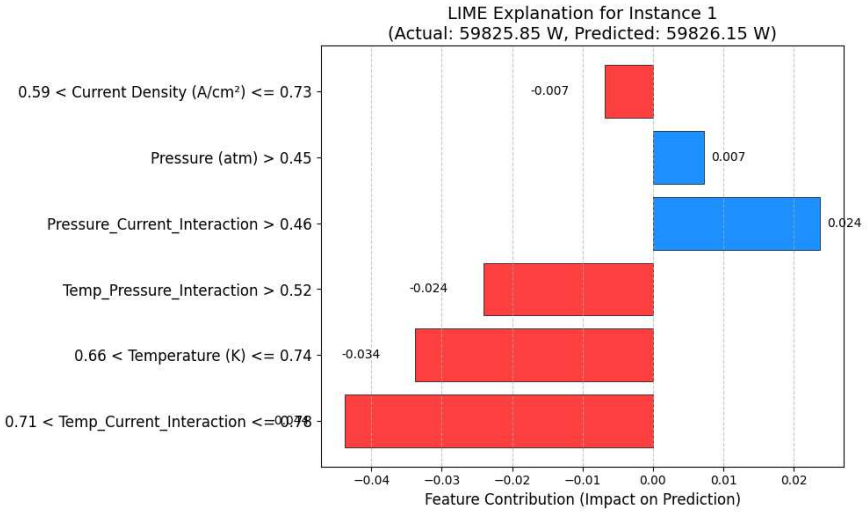

Figure 10: LIME explanation for Instance 1, showing feature contributions to the prediction of Stack Power (Actual: 59822.85 W, Predicted: 59826.15 W).

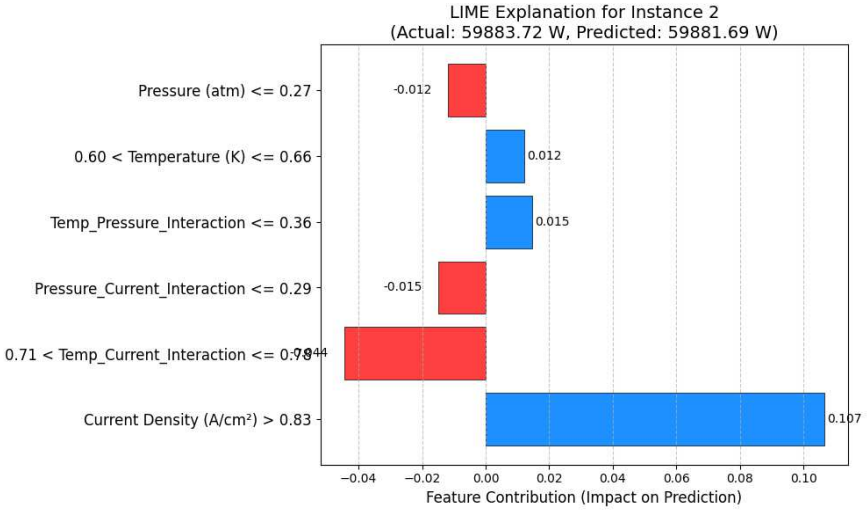

Figure 11: LIME explanation for Instance 2, showing feature contributions to the prediction of Stack Power (Actual: 59883.72 W, Predicted: 59881.69 W).

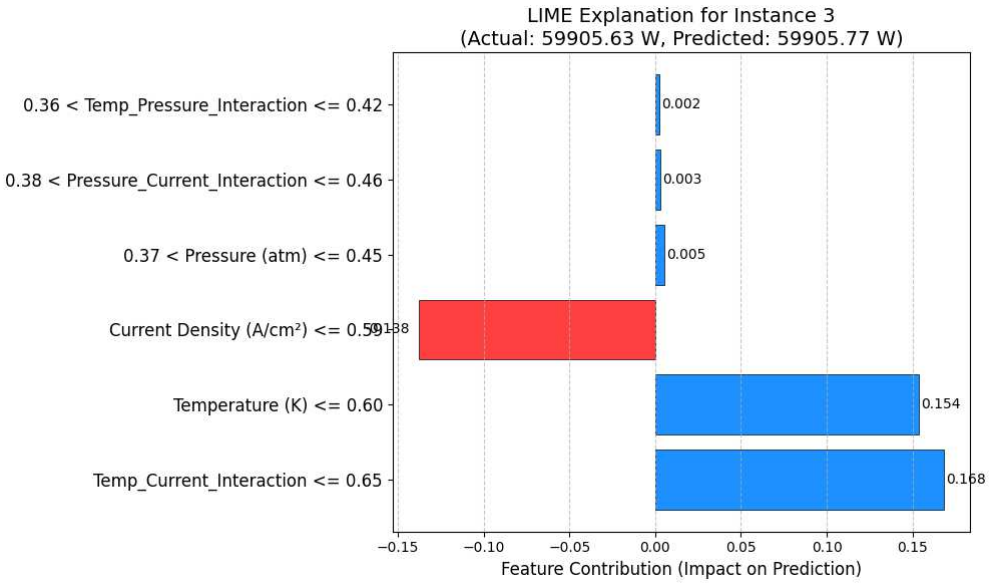

Figure 12: LIME explanation for Instance 3, showing feature contributions to the prediction of Stack Power (Actual: 59,905.63 W, Predicted: 59,905.77 W).

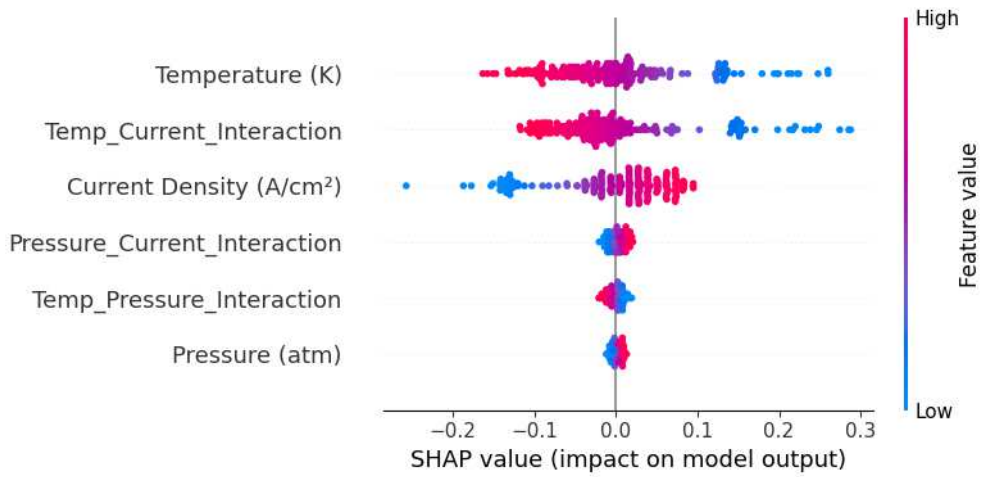

Figure 13: SHAP summary plot illustrating the distribution of SHAP values across the first 200 test instances, with Temperature (K) showing the largest positive impact on Stack Power predictions.

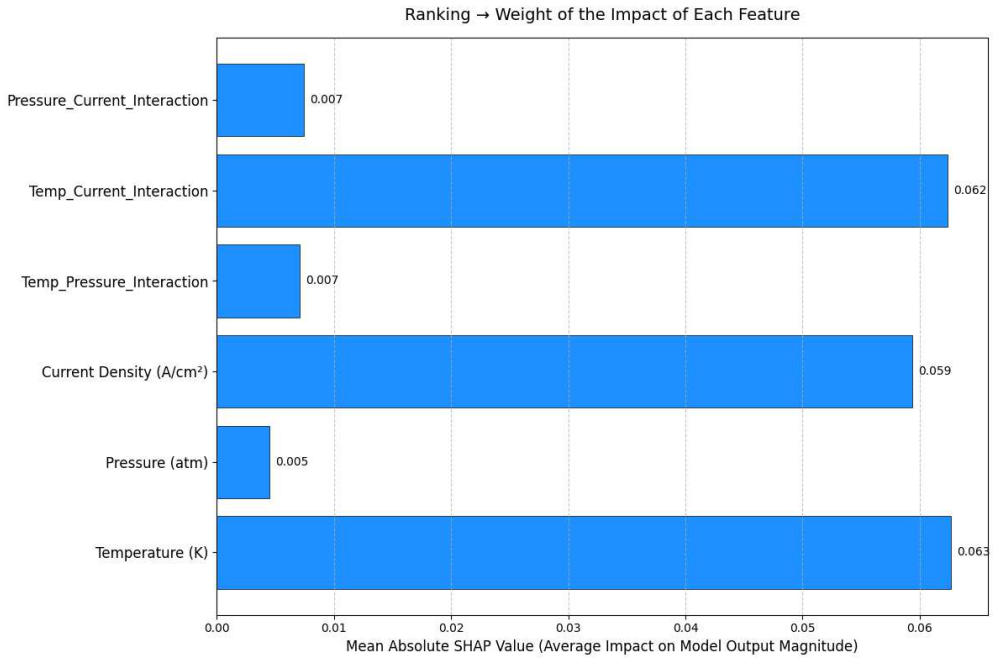

Figure 14: Ranking of features by mean absolute SHAP value, showing the average impact on model output magnitude (Temperature (K): 0.063, Temp_Current_Interaction: 0.062, Current Density (A/cm^2): 0.059, etc.).

3.4 Broader Implications and Real-World Applications

Combining computational modeling with machine learning shows great possibilities to improve energy systems. The PEM fuel cell design results show a strong basis for knowledge and optimization of fuel cell performance. Real time monitoring and control systems made feasible by the TS Mixer model allow fuel cells to be more dependable and efficient in real life by means of prediction of the future.

This work has major implications for the possible use in other energy systems. Even battery management systems: the approaches used here may be modified to forecast and maximize performance in solid oxide fuel cells, hybrid renewable energy configurations [55]. Combining data-driven models with theoretical frameworks can significantly increase the operational efficiency of these systems.

Furthermore, digital twin systems can incorporate the predictive framework this work produced. [56] These systems replicate real time running circumstances, therefore enabling stakeholders to make well-informed decisions on load management, fuel economy, and maintenance. In sectors like transportation, industry, and power generation where sustainability and energy economy take center stage, this capacity is especially important.

This paper provides a comprehensive framework that bridges the gap between computational modeling and machine learning, allowing for the design and optimization of energy systems. The approaches and insights offered here contribute to the larger area of clean energy technology, therefore assisting worldwide efforts to shift to more sustainable and efficient energy systems.

Furthermore, digital twin systems can incorporate the predictive framework this work

produced. [56] These systems replicate real-time running circumstances, therefore enabling stakeholders to make well-informed decisions on load management, fuel economy, and maintenance. In sectors like transportation, industry, and power generation where sustainability and energy economy take center stage, this capacity is especially important.

This paper provides a comprehensive framework that bridges the gap between computational modeling and machine learning, allowing for the design and optimization of energy systems. The approaches and insights offered here contribute to the larger area of clean energy technology, therefore assisting worldwide efforts to shift to more sustainable and efficient energy systems.

4 Conclusion and Future Directions

This study advanced Proton Exchange Membrane (PEM) fuel cell performance by integrating computational modeling with machine learning. A comprehensive thermodynamic and electrochemical model was developed to simulate critical operational parameters, including stack power output, hydrogen consumption, and energy efficiency. The model demonstrated robustness, delivering approximately 60,000 W of power and consuming 3.02 kg/h of hydrogen, closely aligning with theoretical predictions and validating its real-world applicability.

In the predictive modeling phase, the TS-Mixer neural network enhanced real-time monitoring and control. By leveraging engineered feature interactions and robust data preprocessing, the model achieved exceptional accuracy (R^2 score of 0.998, RMSE: 0.571 W, MAPE: 0.00057%). These results underscore machine learning's potential to optimize fuel cell performance, enabling predictive maintenance and operational adjustments.

Future research should build on these findings by incorporating degradation mechanisms, such as membrane thinning and catalyst aging, to enhance long-term performance predictions [10]. Integrating digital twin technology could enable real-time simulations and adaptive control strategies, improving system efficiency. Advanced manufacturing techniques, like 3D printing, may further optimize fuel cell designs for efficiency and recyclability, enhancing environmental sustainability [57]. Extending the computational framework to other energy systems, such as solid oxide fuel cells or hybrid renewable setups, could broaden its impact [58]. Interdisciplinary collaboration across materials science, machine learning, and renewable energy will be essential to unlock the full potential of PEM fuel cells [59].

In summary, this study demonstrates the synergy of computational modeling and machine learning as a transformative approach to advancing PEM fuel cell technology. By bridging theoretical analysis with data-driven optimization, it lays a foundation for smarter, scalable, and efficient energy systems, accelerating the global transition to sustainable energy.

References

[1] S. J. Davis, N. S. Lewis, M. Shaner, S. Aggarwal, D. Arent, I. L. Azevedo *et al.*, "Net-zero emissions energy systems," *Science*, vol. 360, no. 6396, 2018, dOI: https://doi.org/10.1126/science.aas9793.

[2] I. Staffell, D. Scamman, A. Velazquez Abad, P. Balcombe, P. E. Dodds *et al.*, "The role of hydrogen and fuel cells in the global energy system," *Energy & Environmental Science*, vol. 12, no. 2, 2019, dOI: https://doi.org/10.1039/C8EE01157E.

[3] Z. P. Cano, D. Banham, S. Ye, A. Hintennach, J. Lu *et al.*, "Batteries and fuel cells for electric vehicle fleets," *Nature Energy*, vol. 3, no. 4, 2018, dOI: https://doi.org/10.1038/s41560-017-0072-1.

[4] S. Gottesfeld, T. A. Zawodzinski, D. A. Nešić, and X. Li, "Recent advances in PEM fuel cell technology," *Journal of Power Sources*, vol. 392, 2018, dOI: https://doi.org/10.1016/j.jpowsour.2018.04.099.

[5] R. Taccani and N. Zuliani, "Cost and durability challenges of PEMFC flow plates," *Renewable Energy*, vol. 157, 2020, dOI: https://doi.org/10.1016/j.renene.2020.04.147. [Online]. Available: https://doi.org/10.1016/j.renene.2020.04.147

[6] T. Wilberforce, O. Ijaodola, and E. Ogungbemi, "CFD optimization of OPCF flow plates," *International Journal of Hydrogen Energy*, vol. 46, no. 55, 2021, dOI: https://doi.org/10.1016/j.ijhydene.2021.06.121. [Online]. Available: https://doi.org/10.1016/j.ijhydene.2021.06.121

[7] S. G. Kandlikar and Z. Lu, "Two-phase flow dynamics in PEMFCs," *Applied Thermal Engineering*, vol. 195, 2021, dOI: https://doi.org/10.1016/j.applthermaleng.2021.117201. [Online]. Available: https://doi.org/10.1016/j.applthermaleng.2021.117201

[8] B. Zhou, C. Zuo, and F. Ye, "Graded-porosity GDLs for PEMFCs," *Electrochimica Acta*, vol. 403, 2022, dOI: https://doi.org/10.1016/j.electacta.2021.139614. [Online]. Available: https://doi.org/10.1016/j.electacta.2021.139614

[9] G. Zhang, X. Li, and K. Jiao, "Bio-inspired serpentine flow fields," *Energy*, vol. 230, 2021, dOI: https://doi.org/10.1016/j.energy.2021.120841. [Online]. Available: https://doi.org/10.1016/j.energy.2021.120841

[10] Y. Chen, H. Zhang, and Q. Li, "3d-printed PEMFC components for sustainability," *Additive Manufacturing*, vol. 56, 2022, dOI: https://doi.org/10.1016/j.addma.2022.102875.

[11] J. Zhao, Y. Wang, and Z. Li, "Fractal flow fields for PEMFCs," *International Journal of Heat and Mass Transfer*, vol. 202, 2023, dOI: https://doi.org/10.1016/j.ijheatmasstransfer.2022.123715. [Online]. Available: https://doi.org/10.1016/j.ijheatmasstransfer.2022.123715

[12] T. Ghidini, F. Mocera, and A. Somà, "Solar-hydrogen systems for energy resilience," *Applied Energy*, vol. 281, 2021, dOI: https://doi.org/10.1016/j.apenergy.2020.116047.

[13] F. Sun, D. Su, P. Li, and X. Dong, "A novel 3d fine-mesh flow field design and performance analysis for proton exchange membrane fuel cells," *Journal of Power Sources*, vol. 584, p. 233572, 2023, dOI: https://doi.org/10.1016/j.jpowsour.2023.233572.

[14] M. Boudellal, "PEMFC-wind hybrid systems for off-grid power," *Energy*, vol. 254, 2022, dOI: https://doi.org/10.1016/j.energy.2022.124398.

[15] A. Hirsch, S. Derrer, and T. M. Bachmann, "Portable PEMFC systems for electronics," *Journal of Power Sources*, vol. 532, 2022, dOI: https://doi.org/10.1016/j.jpowsour.2022.231348.

[16] O. Schmidt, A. Hawkes, and A. Gambhir, "Fuel cell-powered marine vessels," *Applied Energy*, vol. 278, 2020, dOI: https://doi.org/10.1016/j.apenergy.2020.115639.

[17] D. J. Bents, K. J. Hack, and B. G. Laurent, "PEMFCs in aerospace: NASA's missions," *Aerospace Science and Technology*, vol. 119, 2021, dOI: https://doi.org/10.1016/j.ast.2021.107129.

[18] J. Zhang, X. Li, and H. Liu, "Reactant starvation mechanisms in PEM fuel cells," *International Journal of Hydrogen Energy*, vol. 45, no. 38, 2020, dOI: https://doi.org/10.1016/j.ijhydene.2020.05.132. [Online]. Available: https://doi.org/10.1016/j.ijhydene.2020.05.132

[19] N. Yousfi-Steiner, P. Moçotéguy, and D. Candusso, "Hotspot-induced degradation in PEMFCs," *Journal of Power Sources*, vol. 416, 2019, dOI: https://doi.org/10.1016/j.jpowsour.2019.01.092. [Online]. Available: https://doi.org/10.1016/j.jpowsour.2019.01.092

[20] D. H. Jeon, S. Kim, and J. Lee, "Serpentine vs. interdigitated flow fields," *Energy*, vol. 231, 2021, dOI: https://doi.org/10.1016/j.energy.2021.120867. [Online]. Available: https://doi.org/10.1016/j.energy.2021.120867

[21] J. T. Pukrushpan, A. G. Stefanopoulou, and H. Peng, "Thermal stress in PEMFCs under high-current operation," *Applied Thermal Engineering*, vol. 136, 2018, dOI: https://doi.org/10.1016/j.applthermaleng.2018.03.007. [Online]. Available: https://doi.org/10.1016/j.applthermaleng.2018.03.007

[22] R. L. Borup, J. P. Meyers, and B. S. Pivovar, "MEA degradation mechanisms in PEMFCs," *Chemical Reviews*, vol. 120, no. 15, 2020, dOI: https://doi.org/10.1021/acs.chemrev.9b00458. [Online]. Available: https://doi.org/10.1021/acs.chemrev.9b00458

[23] R. Jilte, R. Kumar, and M. H. Ahmadi, "Phase-change materials for PEMFC thermal regulation," *Energy Conversion and Management*, vol. 267, 2022, dOI: https://doi.org/10.1016/j.enconman.2022.115909. [Online]. Available: https://doi.org/10.1016/j.enconman.2022.115909

[24] C. Tötzke, I. Manke, and N. Kardjilov, "Microchannel cooling in bipolar plates," *Applied Energy*, vol. 302, 2021, dOI: https://doi.org/10.1016/j.apenergy.2021.117541. [Online]. Available: https://doi.org/10.1016/j.apenergy.2021.117541

[25] J. Heo, S. Lee, and H. Kim, "Graphene oxide-reinforced composite membranes," *ACS Applied Materials & Interfaces*, vol. 13, no. 20, 2021, dOI: https://doi.org/10.1021/acsami.1c02431. [Online]. Available: https://doi.org/10.1021/acsami.1c02431

[26] K. Shinozaki, Y. Morimoto, and B. S. Pivovar, "Ultrathin catalyst layers for PEMFC longevity," *Journal of the Electrochemical Society*, vol. 169, no. 4, 2022, dOI: https://doi.org/10.1149/1945-7111/ac63c2.

[27] T. J. Schmidt, B. Binninger, and M. Nachtegaal, "CO and sulfur poisoning in PEMFCs," *Electrochimica Acta*, vol. 318, 2019, dOI: https://doi.org/10.1016/j.electacta.2019.06.097.

[28] A. Iulianelli, A. Basile, and F. Dalena, "Hydrogen purification via molecular sieves," *Renewable Energy*, vol. 152, 2020, dOI: https://doi.org/10.1016/j.renene.2020.01.086.

[29] S. Morando, S. Jemeï, and D. Hissel, "Lessons from the IEEE PHM 2014 data challenge for PEMFC prognostics," *International Journal of Hydrogen Energy*, vol. 42, no. 15, 2017, dOI: https://doi.org/10.1016/j.ijhydene.2016.12.092.

[30] M. Jouin, R. Gouriveau, and D. Hissel, "Accelerated aging tests for PEMFC degradation analysis," *Journal of Power Sources*, vol. 325, 2016, dOI: https://doi.org/10.1016/j.jpowsour.2016.06.015.

[31] D. Banham, S. Ye, and K. Pei, "PtCo catalysts for enhanced PEMFC durability," *Science*, vol. 360, no. 6388, 2018, dOI: https://doi.org/10.1126/science.aar8120.

[32] M. Eikerling, L. Ghassemzadeh, and R. Maric, "Infrared spectroscopy for real-time MEA monitoring," *ACS Applied Energy Materials*, vol. 4, no. 5, 2021, dOI: https://doi.org/10.1021/acsaem.1c00522.

[33] A. Kumar, K. Jiao, and X. Li, "Operando diagnostics for degradation insights," *Journal of The Electrochemical Society*, vol. 168, no. 6, 2021, dOI: https://doi.org/10.1149/1945-7111/ac0c4a.

[34] P. R. Shearing, D. J. L. Brett, and N. P. Brandon, "X-ray tomography of PEMFC components," *Electrochemical Science Advances*, vol. 1, no. 1, 2020, dOI: https://doi.org/10.1002/elsa.202000021.

[35] J. Yang, Y. Wu, and X. Liu, "Proton exchange membrane fuel cell power prediction based on ridge regression and convolutional neural network data-driven model," *Sustainability*, vol. 15, no. 14, 2023. [Online]. Available: https://www.mdpi.com/2071-1050/15/14/11010

[36] W. Huo, W. Li, Z. Zhang, C. Sun, F. Zhou, and G. Gong, "Performance prediction of proton-exchange membrane fuel cell based on convolutional neural network and random forest feature selection," *Energy Conversion and Management*, vol. 243, p. 114367, 2021. [Online]. Available: https://www.sciencedirect.com/science/article/pii/S0196890421005434

[37] K.-Y. Chang, "The optimal design for pemfc modeling based on taguchi method and genetic algorithm neural networks," *International Journal of Hydrogen Energy*, vol. 36, no. 21, pp. 13 683–13 694, 2011, 2010 Asian/APEC BioH2. [Online]. Available: https://www.sciencedirect.com/science/article/pii/S036031991101754X

[38] H.-W. Li, B.-S. Xu, C.-H. Du, and Y. Yang, "Performance prediction and power density maximization of a proton exchange membrane fuel cell based on deep belief network," *Journal of Power Sources*, vol. 461, p. 228154, 2020. [Online]. Available: https://www.sciencedirect.com/science/article/pii/S0378775320304572

[39] I.-S. Han and C.-B. Chung, "Performance prediction and analysis of a pem fuel cell operating on pure oxygen using data-driven models: A comparison of artificial neural network and support vector machine," *International Journal of Hydrogen Energy*, vol. 41, no. 24, pp. 10 202–10 211, 2016. [Online]. Available: https://www.sciencedirect.com/science/article/pii/S036031991530389X

[40] Q. Shuai, Y. Wang, Z. Jiang, and Q. Hua, "Reinforcement learning-based energy management for fuel cell electrical vehicles considering fuel cell degradation," *Energies*, vol. 17, p. 1586, 03 2024.

[41] Q. Tian, H. Chen, S. Ding, L. Shu, L. Wang, and J. Huang, "Remaining useful life prediction method of pem fuel cells based on a hybrid model," *Electronics*, vol. 12, no. 18, 2023. [Online]. Available: https://www.mdpi.com/2079-9292/12/18/3883

[42] J. Zuo, "Ieee 2014 durability test data for pem fuel cells," https://github.com/jianzuo/IEEE-2014-datasets, 2014, accessed: 2025-05-15.

[43] R. O'Hayre, S.-W. Cha, W. Colella, and F. B. Prinz, *Fuel Cell Fundamentals*, 3rd ed. Wiley, 2016, dOI: https://doi.org/10.1002/9781119191766.

[44] Y. Wang *et al.*, "Thermodynamic parameters for pemfc modeling," *Journal of Power Sources*, vol. 435, p. 226830, 2019, dOI: https://doi.org/10.1016/j.jpowsour.2019.03.050.

[45] A. Z. Weber and J. Newman, "PEMFC multi-physics modeling," *Journal of The Electrochemical Society*, vol. 161, no. 12, 2014, dOI: https://doi.org/10.1149/2.0411412jes. [Online]. Available: https://doi.org/10.1149/2.0411412jes

[46] S. Morando *et al.*, "Ieee phm 2014 data challenge analysis," *International Journal of Hydrogen Energy*, vol. 42, no. 11, pp. 7393–7403, 2017, dOI: https://doi.org/10.1016/j.ijhydene.2016.12.092.

[47] D. B. Rubin, "Inference and missing data," *Biometrika*, vol. 63, no. 3, pp. 581–592, 1976, dOI: https://doi.org/10.1093/biomet/63.3.581.

[48] C. Leys, C. Ley, O. Klein, P. Bernard, and L. Licata, "Detecting outliers: Do not use standard deviation around the mean, use the interquartile range," *Journal of Experimental Social Psychology*, vol. 49, no. 4, pp. 764–766, 2013, dOI: https://doi.org/10.1016/j.jesp.2013.03.013.

[49] I.-K. Yeo and R. A. Johnson, "Yeo-johnson power transformation," *Biometrika*, vol. 87, no. 4, pp. 954–959, 2000, dOI: https://doi.org/10.1093/biomet/87.4.954.

[50] J. Han, M. Kamber, and J. Pei, *Data Mining: Concepts and Techniques*. Elsevier, 2011, dOI: https://doi.org/10.1016/C2009-0-61819-5.

[51] S. Chen *et al.*, "Ts-mixer: Time-series mlp architecture," *arXiv preprint arXiv:2303.06053*, 2023, dOI: https://doi.org/10.48550/arXiv.2303.06053.

[52] S. Ioffe and C. Szegedy, "Batch normalization," in *Proceedings of the 32nd International Conference on Machine Learning (ICML)*, 2015, pp. 448–456, dOI: https://doi.org/10.5555/3045118.3045167.

[53] N. Srivastava *et al.*, "Dropout regularization," in *Advances in Neural Information Processing Systems (NeurIPS)*, 2014, pp. 1929–1937, dOI: https://doi.org/10.5555/2627435.2670313.

[54] D. P. Kingma and J. Ba, "Adam: A method for stochastic optimization," *arXiv preprint arXiv:1412.6980*, 2015, dOI: https://doi.org/10.48550/arXiv.1412.6980.

[55] H. Lund, B. V. Mathiesen, D. Connolly *et al.*, "Smart energy and hybrid renewable energy systems," *Energy*, vol. 137, pp. 556–565, 2017, dOI: https://doi.org/10.1016/j.energy.2017.05.123.

[56] A. Rasheed, O. San, and T. Zohdi, "Digital twin: Values, challenges, and enablers," *Computer Methods in Applied Mechanics and Engineering*, vol. 372, p. 113410, 2020, dOI: https://doi.org/10.1016/j.cma.2020.113410.

[57] M. Carmo, D. L. Fritz, and D. Stolten, "Integrating ML and materials science for PEMFCs," *Advanced Energy Materials*, vol. 13, no. 18, 2023, dOI: https://doi.org/10.1002/aenm.202203912.

[58] I. Staffell, D. Scamman, and A. V. Abad, "Interdisciplinary strategies for PEMFC advancement," *Renewable and Sustainable Energy Reviews*, vol. 168, 2022, dOI: https://doi.org/10.1016/j.rser.2022.112742.

[59] International Energy Agency, "Global hydrogen review 2023," 2023, dOI: https://doi.org/10.1787/1225c9a9-en.